An integrated investigation of the Rio tailings - Panasqueira mine (Centre Portugal)

C. Grangeia[1], P. Ávila[1,2], M. Matias[1], E. Ferreira da Silva[1]

[1]GeoBioTec – Geobiosciences, Geotechnologies and Geoengineering, University of Aveiro, 3810-193 Aveiro, Portugal (corresponding author; Email address: cgrangeia@ua.pt);

[2]LNEG –

Abstract

The risks associated with mine tailings have different nature and, thus, only a multiple approach can investigate and monitor comprehensively the characteristics and evolution of mine tailings impacts on the environment.

Deposition at the Rio tailings (Panasqueira Mine) lasted about ninety years. Over one million cubic metres, of complex very fine to fine material, are deposited on a mountain side overlaying the Zezere river, increasing the risk of contamination of one of the most important hydrographic basins in central Portugal.

Herein, a multidisciplinary study including geophysics, geochemistry and borehole information, organized in a GIS, is used to characterize the Rio tailings.

The geophysical survey comprised ERT (Electrical Resistivity Tomography) and GPR (Ground Penetrating Radar) on the mud impoundment, as well as, on the slope of the tailings. The geochemical survey consisted on collecting water and tailings samples, iron coatings, arsenopyrite stockpile material and ferruginous crust. Samples collected in boreholes, drilled specifically for this project, were also analyzed.

The GIS provided imaging of the geophysical, geochemical and particle size spatial distribution, so that comparisons between the different data sets are easily done. Resistivity and GPR allowed bedrock positioning. GPR was able to give layering results within the tailings.

Finally, comparison and correlation between geophysical and geochemical results are carried out and evaluated on the GIS platform.

Key word: mine, geophysics, tailings, geochemistry, contamination, structure, risk

1. Introduction

Mining, like other industrial activities, can impact the environment negatively. Mineral extraction and processing produce crushed and milled waste rock and tailings that cause a potential risk to the environment when exposed to weathering (Dold and Fontboté 2001; Nordstrom and Alpers 1999). About 2.75 billion tonnes of waste has been generated in Europe between 1998 and 2001. Mining and quarrying waste represent 15% of total waste in Western Europe and 31% in former Eastern Europe countries (Eurostat, 2003). In Portugal mining and quarrying activities generated 17 Mt in 2001 which represents 58% of total industrial waste.

Tailing dams have long been associated with mining activity and constitute a major negative impact. Apart from a strong visual impact, other aspects as geotechnical, physical and chemical instability can trigger events with very high negative effects on the environment.

In fact, mine tailing dams are more vulnerable than other retention structures and are a major threat because of their: (1) unstable nature (principally of earth construction), (2) location (often situated near sensitive aquatic ecosystems), (3) large number (in the tens of thousands worldwide), and (4) generally poor to non-existent maintenance (especially after closure of mining activities) (ICOLD, 2001).

Severe accidents have caused casualties and considerable environmental damage resulting in large volumes of tailings being discharged directly into the environment. Recent cases, such as, Aznalcollar

mine in Spain (April, 1998) affecting 2656ha of Donana Nature Park, Baia Mare mine (January, 2000) and Baia Borsa mine (March, 2000) in Romania have clearly shown that, in a short term and environmentally speaking, mine wastes represent a clear and present danger as important as greenhouse gas emissions (BRGM 2001; Puura et al., 2002]

In addition to the risk of catastrophic events, abandoned tailings piles can also release toxic effluents and other potentially hazardous materials into the environment. Ongoing impacts from tailings disposal operations include transport of tailings solids into adjacent environments by wind and water erosion, and pollution of ground and surface water by toxic substances such as dissolved metals, cyanide and sulphates [e-EcoRiskDoW 2001, e-EcoRisk, 2007]. For the past fifteen years many countries have carried out studies on mining and quarrying waste materials in order to respond to the need for scarce natural resources conservation, reducing environmental pollution and conserving energy [Hammond, 1998].

The establishment of a regional information network for the management and decision-support system (*e-EcoRisk*) is a major contributor to the decision-making process of environmental and civil protection agencies charged with the responsibility for assessing, preventing, mitigating, and controlling the potential and actual effects of large-scale industrial spills on the environment. The Panasqueira Sn-W mine was one of the two Portuguese test sites studied in the scope of e-EcoRisk project. According to Ávila et al, 2008 this site was chosen because of: (a) it is an active mine, (b) there are huge tailings piles (the Rio tailings ≈ 1,200,000 m^3 and the Barroca Grande ≈ 7,000,000 m^3) and dams (the Barroca Grande has two mud dams ≈ 1,193,885 m^3 and the Rio tailings has one mud dam ≈ 731,034 m^3), (c) small villages (S. Jorge da Beira, Panasqueira, Barroca Grande and Aldeia de S. Francisco de Assis are located around the mine site, (d) the Zêzere river crosses the area and feeds the Castelo do Bode water dam (located 90 km downstream), the main water supply source for Lisbon and (e) the local population strongly depends on the use of land and water for their subsistence (water supply, agriculture, cattle breeding, fishing, and forestry).

Hence there is need for a better understanding of the environmental problems associated with mine tailings impoundment complex systems and dams in order to monitor them. As the risks are of different nature, only a multidisciplinary approach can fully respond to such a problem. Therefore an integrated approach using Geophysics, Geochemistry and Drilling was carried out and the data were organized in GIS system for a better visualization and overall interpretation and understanding of the Pansqueira Mine Rio tailings deposits.

Geophysics has been used intensively in Environmental problems and in particular in the study of mine tailings problems (Poisson *et al.* 2009). In the investigation of such problems the most frequent techniques used are the Geoelectrical methods (Campbell *et al*. 1999) as the electrical conductivity contrast between the materials contained in mine waste piles and the surrounding rocks is usually large. Moreover, geoelectrical methods may also help to map features inside the waste itself, such as, water table or even variations of the tailings inner structure (Campbell, & Fitterman, 2000). Characteristics such as grain size variation, mineralogy and chemistry differences inside the impoundment, thickness of the tailings, positioning of the underlying sediments, bedrock relief and internal structures (cavities and voids) are suitable targets for the application of geoelectrical methods (Vanhala *et al.* 2005).

Detection of seepage paths in mine tailings is also important since their presence can be a serious threat to tailings integrity. Again in this case, geoelectrical methods play an important role in a comprehensive methodology for the assessment of anomalous seepage conditions (Panthulu *et al*., 2001).

Relations between geophysical and geochemical data have also been investigated (Vanhala *et al.* 2005). The geophysical signature of mine tailing contaminants is dependent on a number of factors including lithology, ground porosity, total dissolved solids and pH of the pore water (Watson, M.I. *et al.*, 2001) and other studies have established correlations between earth resistivity and groundwater chemistry (Ebraheem *et al*., 1990; Yuval, 1996).

The main objectives of the study over the Panasqueira Mine Rio tailings are:

- to characterize the polluting aptitude of sulphide-rich waste contained in the Rio tailing dam through geochemical and mineralogical studies and to establish the potential environmental impact in case of Rio tailing collapse;

- to investigate the use of ground geophysical electrical methods for mapping tailings impoundment internal sediment structures (limits and stratigraphy), seepage and pathway locations, bedrock depth and topography estimates;

- to compare and join interpret geophysical and geochemical features;

- to construct a geographical system platform for management and risk assessment of the Rio tailings impoundment dam.

2. Site Description

The Panasqueira mine - Rio tailings (lat: 40º07'32.71''N, long: 7º42'51.18''W) is near the town of Covilhã, Central Portugal. Local topography ranges from 350 to 1080 m with deep valleys (Reis 1971). Streams are generally dry in the summer and flooded in the winter. Climate is aggressive in the region, hot and dry during the summer and cold, rainy and windy in the winter. The average annual rain precipitation is 1600 mm and snow falls frequently above the altitude of 700 m. The average annual temperature is 12º C, values ranging from 0 ºC in the winter to about 30ºC in summer. Evapotranspiration is around 1080 mm (www.inag.pt).

2.1. Panasqueira Mine Brief Geology and Mineralization

Panasqueira Mine deposit is located in the so called Central Iberian Zone (CIZ; Figure 1).

Colocar aqui a figura em falta

Figure 1: Synthetic map showing the location of Panasqueira mining area and the Rio tailing, the main geological units (Farinha 2005) and location of

The Panasqueira ore deposit is a typical example of a Sn-W hydrothermal mineralization associated with the Hercynian plutonism. The mineralized zone has an average length of 2500 m, width ranging from 400 to 2200 m and extends, at least, 500m in depth (Cavey and Gunning 2006). Panasqueira Mine has been active for over 100 years and is one of the largest economic vein deposits in the world. During the period 1947-2001, over 27 million tonnes of rock has been mined, produced approximately 92,800t of tungsten concentrate, 4,800t of tin concentrate and 28,600t of copper concentrate (Smith 2006).

The Panasqueira deposit consists of a series of stacked, sub-horizontal, hydrothermal quartz veins intruding into the Beira schists and shales. The paragenesis is complex and four stages of mineral formation are generally accepted: 1) oxide-silicate phase [quartz, wolframite; cassiterite]; 2) main sulphide phase [pyrite, arsenopyrite, pyrrothite, sphalerite, chalcopyrite]; 3) pyrrothite alteration phase [marcasite, siderite, galena, Pb-Bi-Ag sulphosalts]; 4) late carbonate phase [dolomite, calcite] (Breiter 2001; Corrêa de Sá et al. 1999; Correa and Naique 1998; Noronha et al. 1992).

The commonest minerals are quartz, wolframite, pyrite, pyrrhotite, arsenopyrite, chalcopyrite, cassiterite, beryl, mica, and fluorite. However, Panasqueira mine has many rare minerals that can only be observed microscopically, making it a site of some scientific importance. More than 65 minerals, including sulphides, sulphosalts, oxides, carbonates, silicates, phosphates, and tungstates minerals, have been identified (Kelly and Rye 1979).

2.2. Mining Activity and Potential Environmental Considerations

Historical data shows that Romans worked the area for tin. The first prospecting licence was granted in 1886 and the first reference to wolframite mineralization dates from 1888 (Cavey and Gunning 2006).The Panasqueira mining concession covers an area larger than 2000 ha and since 1928 is exploited by Beralt Tin and Wolfram Lda. (Corrêa de Sá et al. 1999). The first mining works were opened at Cabeço do Pião (Rio) and then moved to the Panasqueira village and other places as richer mineral occurrences were found. Thus, exploitation extended to other areas (Barroca Grande, Corga Seca, Panasqueira, Rebordões, and Vale da Ermida).

The economic exploitation has been focused mainly on wolframite, cassiterite, and chalcopyrite, the last two as by-products. On average, the “tout-venant” contains 0.3% WO_3 and the three final concentrates are recovered with 75% WO_3, 72% SnO_2, and 22% Cu together with significant amounts of Ag.

The long history of exploitation and ore treatment operations are testified by the presence of tailings and other debris in Vale de Ermida, where old infrastructures, as well as, large tailings piles from the earliest years of production (late 1890’s to 1927) can be found. These were abandoned and a new plant was constructed at Rio (Cavey and Gunning 2006). When exploitation works moved to Barroca Grande, the ore was transported along a 4 km cableway to the concentration plant in Rio. The plant and tailings disposal were finally deactivated in 1996.

Nowadays, exploitation is focused at Barroca Grande and Panasqueira is an underground mine using highly mechanized room and pillar methods. Mine waste is deposited in the large Barroca Grande tailings area (Ávila et al., 2008).

During the mining process, two types of mine waste are generated:

- coarse aggregates from rock blasting that, since 1970s, have been used as a by-product for bituminous mixtures or disposed in tailings;

- waste mud from the concentration plant that is conveyed by pipelines into lagoons built specifically for that purpose (several million tonnes have been deposited and almost 100 t are being added each day).

The waste is rejected after the ore treatment process. This process begins with heavy media separation (HMS) for the coarse fractions of material. In a second phase, cyclones produce ore concentrates with high metal content, and gravitic tables are used to treat the sands. These pre-concentrates contain all the existent heavy minerals, such as wolframite, cassiterite, sulphides, and siderite. Until 1996, these pre-concentrates were transported to the Rio plant, but today, the final separation procedures are carried out in Barroca Grande exclusively. James flotation tables are used for the pre-concentrates. The floated sulphides constitute the steriles and feed the so called copper circuit. Copper concentrates are recovered after differential flotation in Denver cells (Corrêa de Sá et al. 1999; Reis 1971; Rodrigues and Gonzalez 1973). It must be emphasised that arsenopyrite (the main sulphide present) is rejected with the tailings that contain about 30% As.

The Rio tailing site, located near and draining directly to the Zêzere River, is a large site where tailings have been disposed of for approximately 90 years. Historical records show that tailings deposition started around 1905-1910 and finished in 1996. There is scarce information about old tailing consolidation structures, particle size distribution, material composition and spatial distribution. Topographic data were gathered and old blueprint topographic maps were digitized so digital terrain models were produced. Figure 2 depicts digital elevation models obtained by digitizing the underlying original topography (A), and actual surface (B) from the topographic survey. 3D perspectives are shown at the lower part of Figure 2; original topography (C) and actual surface topography (D).

Locally, altitudes vary from 351 m (Zêzere River valley) to 636 m at the top of the mountain. Rio tailings slope are dipping at about 35º and average heights are about 90m. Two water lines are identified and drawn over the Figure 2A (dashed lines). Due to its shape, depth and extension they have an important role on the stability of the mud impoundment and tailings.

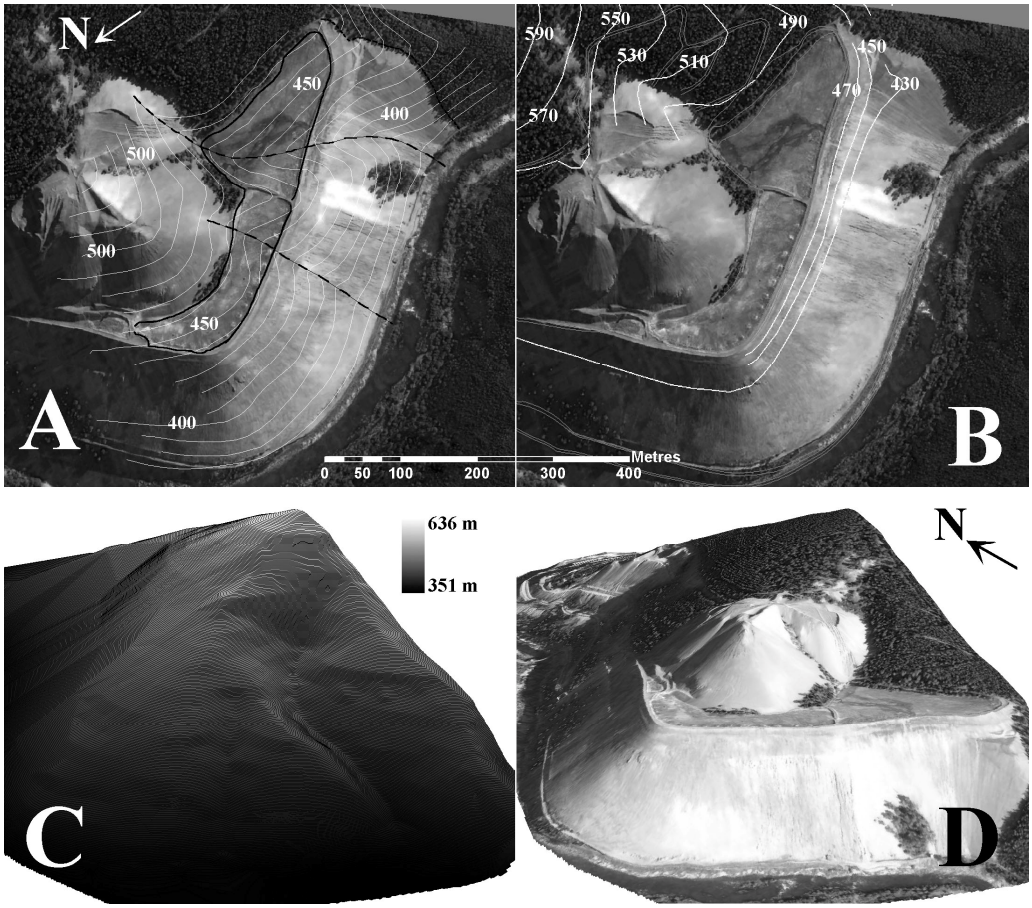

Figure 2: Digital elevation model and 3D perspectives of the Rio mine tailings area.

3. Field Survey

The field survey at the Rio tailing consisted on:

- A geophysical survey on the slope and at the top of the tailings using ERT and GPR. These techniques have been used with success to delineate geometrical features and near surface heterogeneities, to detect seepage paths for safety evaluation and to provide data to be compared with geochemical data as it has been mentioned in the literature (Campbell *et al.*, 2000, Panthulu *et al*., 2001, Poisson *et al.* 2009, Sjödahl *et al.* 2005, Van Dam *et al.*,2005, Vanhala *et al.* 2005,).

- A geochemical survey based on the collection of samples in four boreholes, tailing samples, water samples, iron coatings, arsenopyrite stockpile material, ferruginous crust, surface waters and subsequent analysis. These are considered to be the most representative of the surface environment, and are commonly used in environmental geochemical investigations bibliografia. Sample positioning used GPS and was geo-referenced to UTM coordinates.

All information was gathered in a GIS project so that spatial relations between data and interpretation were easily understood.

3.1 Geophysical Data Aquisition

The geophysical survey consisted on Ground Probing Radar (GPR) profiling and Electrical Resistivity Tomography (ERT). Figure 3 shows the location of the survey.

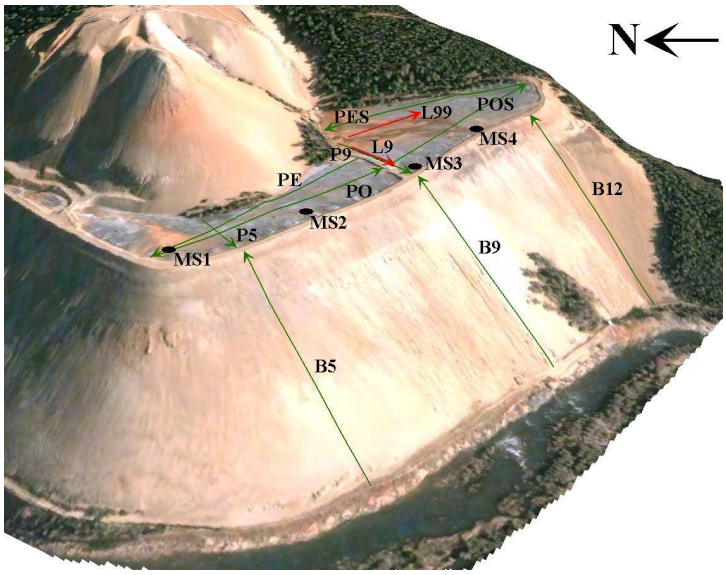

Figure 3: Perspective (3D view) of the geophysical survey: Green - GPR profiles; Red - dipole-dipole profiles.

The ERT survey, on the top of the tailings, consisted on two electrical data profiles, L99 and L9, using a dipole-dipole array, Figure 3. Profile L99 has a total length of 76 m, after inversion, whilst profile L9 is 52 m long. Electrode positioning, and field operations in general, were difficult because of the very dry and stiff surface. The L99 ERT profile used a maximum *n* value of 8 and L9 a maximum *n* of 6. The equipment used was a Syscal R1 Plus resistivity meter.

The GPR survey was carried out on the top of the tailings (mud impoundment), that is, profiles PE, PO, P5, P9, POS, and PES. Further GPR data profiles B5, B9 and B12 were acquired down the slope of the tailings. Figure 3 depicts the acquisition direction for all profiles and Table 1 shows GPR profile lengths.

Table 1: GPR profile lengths

GPR profile	Total length (m)
PE	216
PO	220
P5	52
P9	87
PES	207
POS	209
B5	184
B9	186
B12	200

GPR field operations were adapted so that a continuous survey was possible. Therefore, continuous GPR data acquisition was only possible by fixing the equipment on a rubber rug pulled by a control velocity mine winch at a fixed velocity. This way it was possible to obtain GPR data uphill over the tailings slope. The same equipment and procedure was used to get data from the mud impoundment surface to speed up operations without loss of quality data.

All GPR data was acquired using a PulseEkko IV with a 100 MHz unshielded antenna, in bi-static mode, 1.2 m antenna separation, 200 ns time window, 1.25 GHz sampling frequency and 0.1 m trace increment.

3.2 Geochemical Data Acquisition

3.2.1 Sampling

Samples from Rio tailings were used to establish the granulometric and mineralogical characteristics of its materials, as well as, to investigate geotechnical and hydrological behaviour, that is, stability,

landslides, formation of ravines, erosion, water circulation at the surface, resurgences, etc. For those proposes selected samples from four available boreholes,MS1 to MS4 – Figure 3, (Dinis da Gama 2002) were used. Technical data for all boreholes are given in Table 2, as well as, the depth of the samples (relative to the top of the borehole).The cores are 30 cm long and were collected by the Bonne Esperance probe referencia (I.G.M.).

Table 2: Borehole data information.

	Borehole identification			
	MS1	MS2	MS3	MS4
Surface Orientation	S40ºW	-	-	S40ºW
Inclination	-45º	Vertical	Vertical	-45º
Length (m)	43.58	21.95	34.63	40.13
Core diameter (mm)	123	123	123	123
Depth of Sample 1 (m)	2.39	2.73	2.32	2.32
Depth of Sample 2 (m)	10.00	13.48	8.00	8.00
Depth of Sample 3 (m)	23.00	19.58	16.53	16.53
Depth of Sample 4 (m)	35.49	-	32.00	32.0
Depth of Sample 5 (m)	40.43	-	-	36.00

One iron coating sample was collected in Zêzere River, just downstream of Rio tailings (near stream sediment sample Zss12A) and a ferruginous crust sample in the basement of Rio tailing (near surface water SW10).

Further surface water samples were collected. Thus, samples SW4 and SW4A were collected from the Zêzere River, upstream of the Rio tailings (local background samples); sample SW6 was collected from the Zêzere River but downstream of both tailings areas (Barroca Grande and Rio); samples SW10, SW11, and SW12 are seepage waters collected at the base of the Rio tailings dam.

All samples were collected using a clean 1 L acid-washed polyethylene bottle and stored at 4ºC until analysed.

3.2.2 Sample Preparation

Tailings and drilling core samples were oven dried until dryness before dry sieving at 40ºC, mixed, homogenized and sieved through a < 200 mesh screen for chemical analysis. In order to analyze the dissolved phases, 250 ml of surface waters from each sample was filtered on-site through 0.45µm Millipore membrane filters using an all-plastic pressurized filtering system (ASTM 1984). Samples for metal analysis were immediately preserved after collection in the field, with pH reduction to 2.0 using HNO_3, avoiding Fe hydroxide precipitation. All the water samples were stored at 4ºC pending further analysis.

3.2.3 Sample Analysis

At each site, temperature, pH, and electric conductivity (SC) of the surface waters were recorded. The pH was measured with a previously calibrated HI 8424 microcomputer pH meter. Conductivity was measured using a HI 8633 microcomputer electric conductivity meter. All SC measurements have been referenced to 25ºC. HCO_3 concentration was determined *in situ* by volumetric titration on filtered unacidified samples with sulphuric acid.

Chemical analyses of the homogenized stream sediments, tailings and dam samples were carried out in an accredited lab. For trace metal analysis, a 0.5 g split was leached in hot (95ºC) *aqua regia* (HCl-HNO_3-H_2O) for 1 hour. Although not all minerals are decomposed during the *aqua regia* digestion, these results obtained for heavy metals are considered as total concentrations. After dilution to 10 ml with deionized water, the solutions were analyzed for Ag, As, B, Ba, Be, Cd, Co, Cr, Cu, Fe, Mn, Mo, Nb, Ni, P, Pb, Sb, V, Y, and Zn (by conductive plasma emission spectrometry). The Sn and W were analysed separately by X-ray fluorescence (XRF), since the high stability of the XRF system generally allows the accurate analysis of Sn and W. The detection limits were based on three times the standard deviation of a reagent blank that was analyses ten times. The accuracy and analytical precision were determined using reference materials (SO1, SO2, SO3, SO4, FER1, FER2, FER3, and FER4 from the Canadian Centre of Mineral and Energy Technology; PACS-1 from NRS26 CNRC; and 2711 from NIST) and duplicate samples in each analytical set. The results were within the 95% confidence limits

of the recommended values given for this certified material. The relative standard deviation was between 5 and 10%.

Surface water samples were analyzed without pre-concentration. The analyzed elements include major anions (Cl^-, NO_3^-, and SO_4^{2-}), major cations (Ca, K, Na, and Mg), as well a suite of dissolved trace metals (Ag, Al, As, Bi, Cd, Co, Cu, Fe, Hg, Mo, Ni, Pb, S, Sb, and Zn). Unacidified samples were analyzed using a Dionex 1000i ion chromatography (IC) Work33 station to determine the chloride, nitrate, and sulphate concentrations. Anisocratic elution with a sodium bicarbonate–sodium carbonate eluent was employed together with a Dionex AS4-SC column. Although standards were prepared containing the above anions only, other anions would have been detected, if present, at levels greater than ≈ 0.1 mg L^{-1}. For concentrated samples, dilution was required for reliable anion analysis. The concentrations of major cations and trace elements in acidified waters were determined using mass inductive plasma spectrometry (ICP-MS) at the same accredited lab. Reagent blanks and duplicate samples were inserted into each batch for quality control (Ramsey et al. 1987). The geostandards AQUACHECK and EAA 4 were used to check the validity and reproducibility of the results. Depending on the concentration levels, typical uncertainties, including all error sources, are less than 6% for the trace elements, and between 2% and 7% for the major anions. The limit of detection for the analyzed trace metals is about 0.05-10 mgL^{-1}.

The mineralogical analysis consisted on the identification of the mineral constituents in selected solid media samples (including efflorescences) by X-ray diffraction. The mineralogical composition was determined using a Philips X'Pert MPD equipment equipped with CuKa radiation, graphite monochromator, automatic divergence slit, and 0.5-receiving slit. Step size of 0.05º 2θ, scan setting of 2-70º 2θ, and 10 s counting times were chosen.

4. Results and Discussion

4.1 Geophysical Data Processing and Interpretation

4.1.1 GPR

GPR processing was done using dedicated commercial software (Sandmeier's Reflex-Win). Data processing consisted on: Set time zero, First arrival correction, DC removal, Dewow, Background removal, BandPass filtering and energy decay gain. Time - Velocity conversion was achieved by hyperbola velocity fitting analysis in GPR profiles.

In spite of using energy decay gain, GPR profiles (P5, P9, PO and PES) revealed high data attenuation, as it could be expected because of the nature of the media. Nevertheless, GPR profiles on the slope of the tailings showed significantly lower energy loss, herein just shown the B9 GPR section. This is due to the material size distribution over the tailings, that is, the mud impoundment on the top of the tailings is composed by very fine materials, whereas gravel materials are dominant on the slope of the tailings.

4.1.2 GPR Profiles on the Mud Impoundment – Top of the Tailings

Mud waste mine materials have been transported, in liquid phase, by pipes, and deposited on the surface. Therefore, it is expected horizontal to sub horizontal bedding signatures and, due to several deposition time episodes, interbed crossing.

The surface laying materials consist of complex polymetallic sulphides mine waste, with low Ph values. Hence, high conductivity, low signal penetration, was expected and observed on most of the radargrams (Figure 4, Figure 5 and Figure 6). Consolidated hard crusts detached from the surface were found and difficult to avoid in the GPR survey. This has caused antenna coupling problems and their negative signal effects are frequently observed in GPR data (Figure 4 and Figure 6).

Some GPR profiles carried out on top of the tailings are presented to give an overall account of the GPR response, particularities and benefits in these circumstances.

4.1.2.1 GPR profiles P5 and P9

Figure 4 shows P5 and P9 radargrams (top) and their proposed interpretation (bottom). These profiles, located on the top of the tailings, Figure 3, are parallel to each other and have the same acquisition direction. Both radargrams, P5 and P9, have the same general pattern features, although GPR profile P9 shows a better signal penetration. This is in accordance with the observed difference in surface water content for both places. The interpretation, bottom of Figure 4, proposes three main event signatures:

(a) interfaces between datasets, presented as grey thicker lines; because of the complexity of the media these interfaces are often discontinued. They are interpreted as layering events different from bedding due to time interval deposition, major mud waste volume deposition, or simply by change in the material type deposition;

(b) ring down effects starting at time zero, interpreted as bedding and presented as shorter black lines;

(c) other closed black lines, starting later in time, identified as antenna ringing possibly due to voids. It is possible that the consolidated hard detached crusts are present also in depth. This could be explained by dried mud crusts as the mud impoundment has grown with deposition.

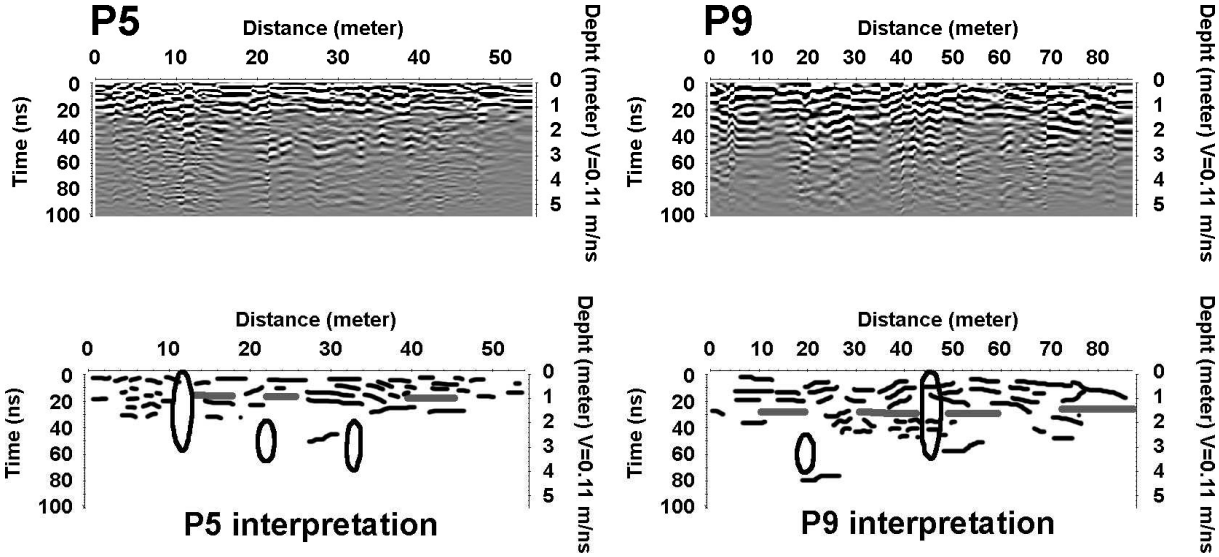

Figure 4: Radargrams P5 and P9 (Top), P5 and P9 proposed interpretation (Bottom). Grey lines - major bounding surfaces between strata sets, black lines - bedding and black areas correspond to Antenna ringing (coupling) and ring down effect (voids).

4.1.2.2 GPR profile PO

The interpretation of the GRP profile PO is depicted in Figure 5, radargram on top and proposed interpretation on the bottom. This profile was carried out the edge and over the western part of the tailings, Figure 3.

In general, the radargram displayed in Figure 5, shows low signal penetration depth (maximum depths up to 1.5 metres), approximate horizontal to sub-horizontal strata bedding and two attenuation zones at each side of a central part of the radargram.

Three main events are interpreted: first the grey thicker lines that could be associated with major bounding surfaces between strata sets; second, strata sets bedding identified with black thinner lines and, finally, ring down effects represented as closed black lines.

At the centre of the radargram and closer to the schist bedrock, higher signal penetration is visible by the identification of deeper strata events. At both sides from this central position, away from the schist bedrock, there is a decrease in signal penetration. Again, at the radargram beginning, near the edge of the slope, it is possible to identify deeper events, which may be related to a dry, higher resistivity and lower attenuation area. Unfortunately, because of the high attenuation it was not possible to identify the schist bedrock.

Bounding surface events are identified by major angle discontinuities. They are closely spaced and have some lateral continuity. Between these, low angle depositional bedding is visible. These features are in close agreement with the known deposition processes of waste mine materials. Inter-bedded crossing was not possible to convenient interpret since there were no close parallel GPR profile for the necessary interpretation support.

Ring down effects are also present in Figure 5. The proposed interpretation (bottom of Figure 5), depicts some of these major events. The observed, thick and detached from surface, hard mud crusts, are often associated with these effects, as they cause inefficient antenna coupling, but the presence of a shallow water table can also be responsible for such effects. These events should start at early (since time zero) registry time within the GPR radargram.

Ring down effects can also develop later in time. In this case it is likely that voids, as well as, changes in material electrical properties can be responsible for high electromagnetic impedance contrasts and cause ring down effects in radargrams. This signature is registered later in time as it is the case in the proposed interpretation of Figure 5.

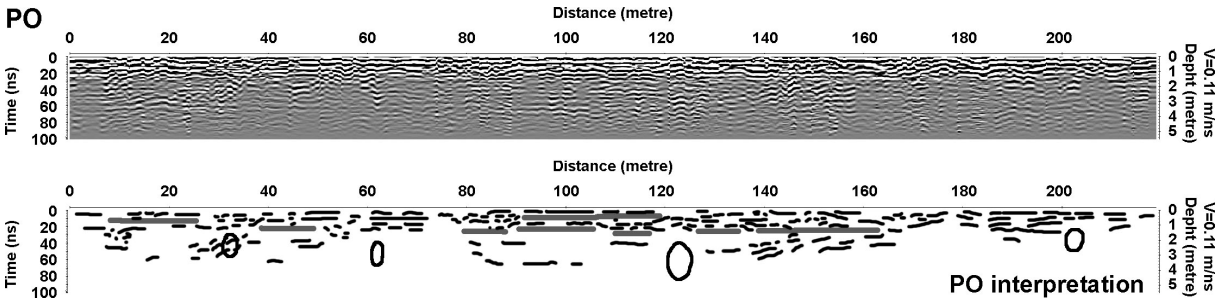

Figure 5: PO radargram (top) and proposed interpretation (bottom). Grey lines - major bounding surfaces between strata sets, black lines - bedding and black areas correspond to ring down effect (possibly voids).

4.1.2.3 GPR profile PES

PES radargram is depicted in Figure 6. It corresponds to data gathered on the Eastern part of the top of the mud impoundment, far from the slope of the tailings and near the schist bedrock. It shows a more pronounced attenuation zone at the end (starting at 180 metres). Penetration depth is about 1.5 m as in PO GPR profile (Figure 5), but the events separation is clearer. Major bounding surfaces are depicted in grey thicker lines, whilst strata bedding as thinner black lines. Both show sub-horizontal low angle deposition, as expected.

Ring down effects are depicted as black closed lines. The proposed interpretation shows only two events, one, starting at time zero, that should correspond to antenna coupling inefficiency (antenna ringing), and a deeper event that could be the result of a void. In general, strata bedding is in agreement with the known signatures for the materials deposition and mud impoundment deposition.

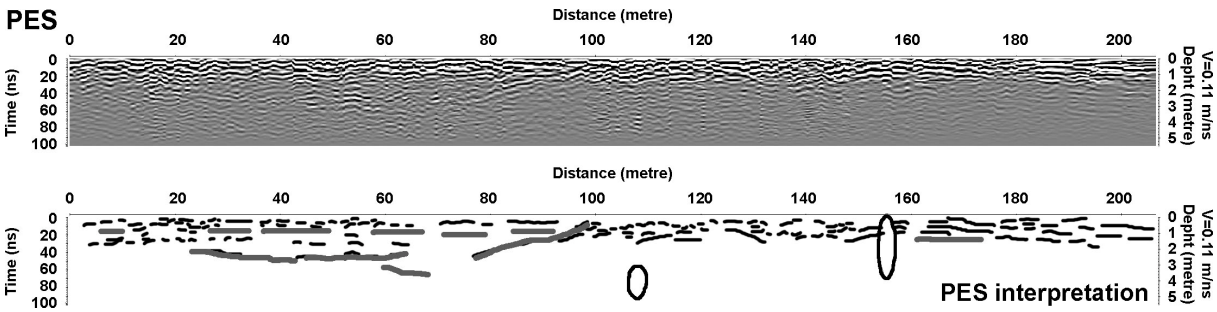

Figure 6: PES radargram (Top) and proposed interpretation (Bottom). Grey lines - major bounding surfaces between strata sets, black lines - bedding and black areas correspond to Antenna ringing (coupling) and ringdown effect (voids).

4.1.3 GPR profiles on the tailings slope

4.1.3.1 GPR profile B9

GPR profile B9, Figure 7, is located at the middle of the slope tailings near a small schist outcrop, it was chosen as representing the survey carried out uphill and on the slope of the tailings. The starting position (zero m) of the radargram corresponds to the lower part of the tailings, Figure 3.

The bottom of Figure 7 shows the proposed interpretation. Four types of events have been interpreted: (1) the thicker black line depicts the schist bedrock bounding surface; (2) the grey lines are interpreted as major bounding surfaces between strata sets; (3) the thinner black lines are interpreted as bedding and (4) the closed black line is interpreted as an area affected by antenna ringing due to inefficient antenna coupling.

Starting a hundred metres uphill it is possible to distinguish two major attenuation areas. A small area showing some signal attenuation and the second much closer to the mud impoundment that shows higher signal attenuation. This higher attenuation can be explained as the waste deposition processes that usually separates coarse grain material at the base from finer material at the latest stages at the top (Van Dam, R.L.,2005).

Near the surface, top of the radargram - Figure 7, layering is parallel to the surface. This signature changes and from the proposed interpretation (bottom of Figure 7), it is more visible towards the end and at larger depths of the GPR profile.

On the left part of the radargram, there are other features showing some degree of angle discontinuity. They are interpreted as early deposition bedding events over the schist bedrock itself. There is also some irregularity on the spacing of the major bounding surfaces that can be explained by the apparent bedding angle, irregular time deposition, volume deposition or even material deposition. It is also possible that there could be some man made supporting structure responsible for the observed features.

The top of the schist bedrock provides a strong signal response. Hence, there is a clear material differentiation. This could be explained by material migration mechanisms such as water transportation, gravity or even wind in the beginning or during the pilling up of the tailings over harder and impermeable schist bedrock.

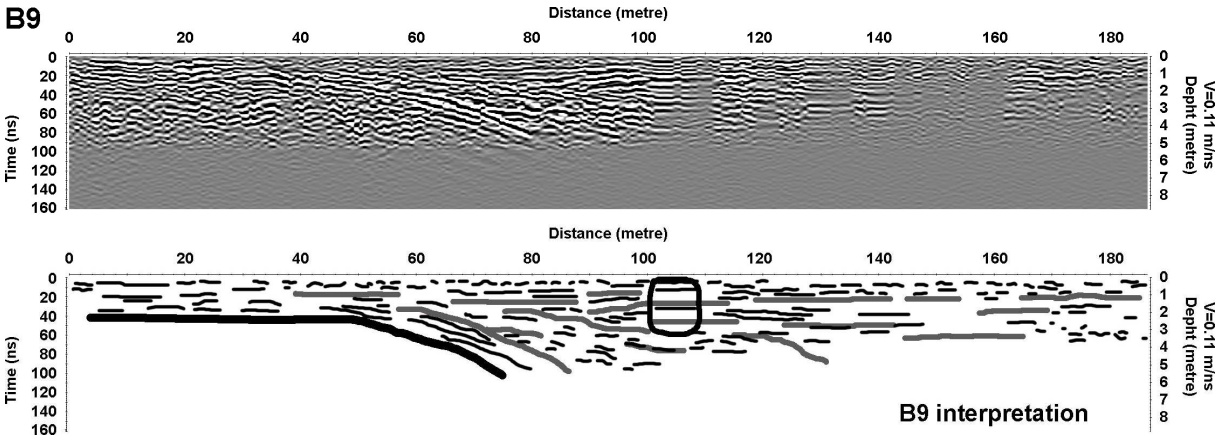

Figure 7: B9 radargram (top) and proposed interpretation (bottom). Grey lines - major bounding surfaces between strata sets, thick black line - Bedrock interface, thinner black lines - bedding and black areas correspond to Antenna ringing (coupling).

Figure 8 shows a photography (top) of a vertical rupture section (20 m by 3 m) of the tailings and the corresponding interpretation scheme (bottom) to illustrate the inner structure of the tailings. The thick black lines depict major bounding surfaces between data sets and bedding is represented by the thinner black lines; the grey thin lines mark the eroded area limits on the vertical section.

This direct interpretation of an observed field section confirms that bounding surfaces and bedding are in agreement with the GPR interpreted sections and expected depositional signatures for these materials in the tailings.

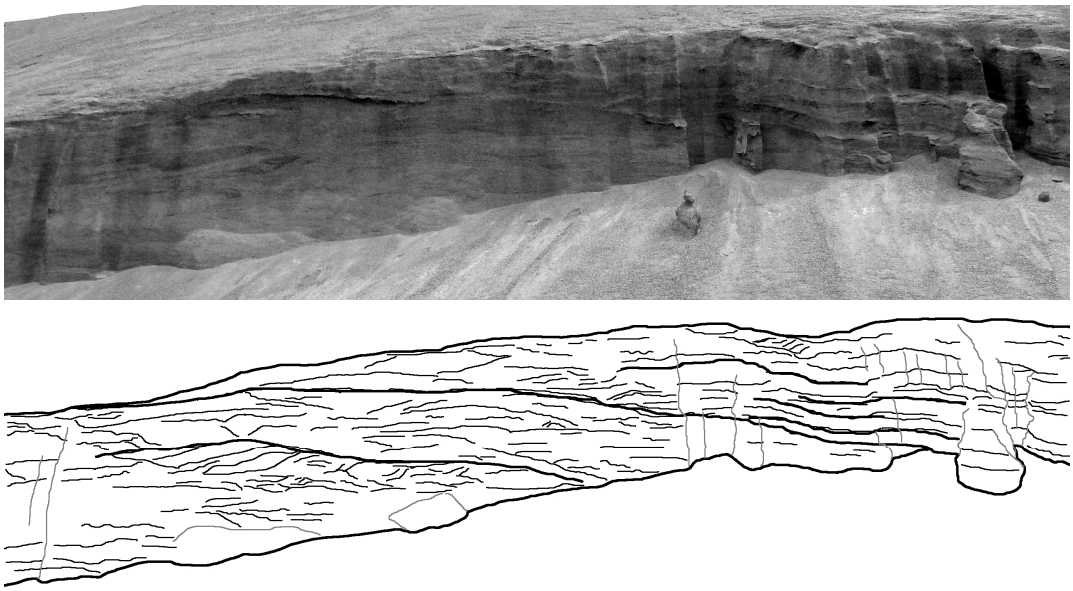

Figure 8: Photograph of a vertical rupture of the tailings (top) and the corresponding bedding identification (bottom).

4.1.2 ERT

Two ERT profiles were carried out, L99 and L9 (Figure 9 and Figure 10), to investigate heterogeneities in the mud impoundment materials, as well as, to locate schist bedrock under the tailings.

L9 is located at the centre of the tailings (Figure 3) and is 52 m long. The profile started near a schist outcrop and ended near the slope of the mud impoundment. On the other hand, L99, 76 m long, is located on the eastern area of the mud impoundment (Figure 3) and crosses over an expected water line under the tailings.

ERT field data were inverted to generate two dimensional distribution models of resistivity using Res2DInv (Loke 2000; Loke and Barker 1996). L99 (Figure 9) has a RMS error of 1.59% at iteration 10, whilst L9 (Figure 10) has a RMS error of 3% for the same iteration number.

The inverse model resistivity section for the L99 profile is shown in Figure 9. Three main distinctive zones are proposed. A first one, with high resistivity, dipping gently westwards, is interpreted as the schist bedrock contrast limit. On the western part of the section (left side of Figure 9), it is identified a very low resistivity area. It should be positioned over the expected buried water line and, hence, in close relationship with a higher water content. Comparatively, the eastern part of the section (right side of Figure 9) shows higher resistivity values, that probably correspond to deposited materials with lower water content. Mud material composition changes, in particular size distribution, can also contribute to the differentiation between East and West zones (right and left side of Figure 9).

Apart from major resistivity changes it is possible to identify horizontal resistivity continuity by opposition to resistivity vertical changes. This should correspond to horizontal / sub-horizontal layering material deposition on the mud impoundment.

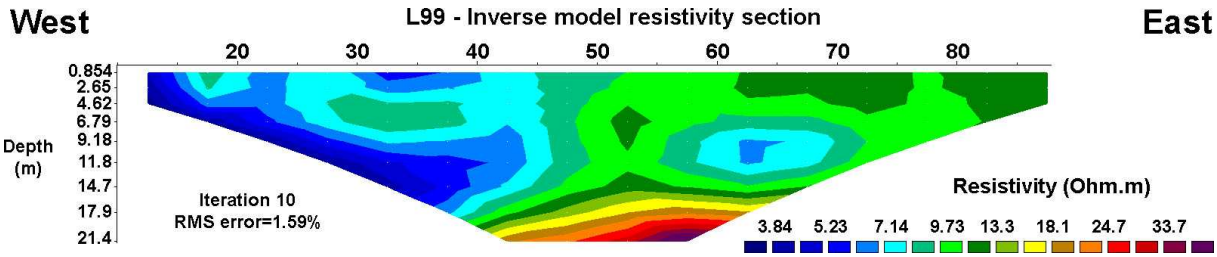

Figure 9: L99 profile - Inverse model resistivity section

When internal erosion occurs, fine particles are washed out, porosity increases and so with the water content which decreases resistivity, afterwards the loss of fine particles will lead to an increase of resistivity (Sjödahl P., *et al.*, 2007). The observed resistivity distribution above the filled water line (Figure 9) is compatible with a seepage pathway.

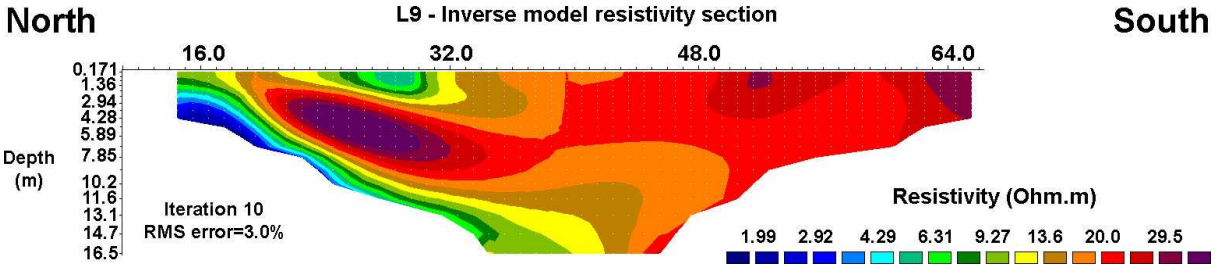

Figure 10: L9 profile - Inverse model resistivity section

The ERT L9 inverse model resistivity is shown in Figure 10. Generally, high resistivity values are displayed near the tailings slope (right side - south) whilst lower resistivity values are present at the northern part of the section (left side - north). Between positions 16 and 32m, at depths ranging from about 3 to 10 metre a high resistivity zone is modeled.

Spatial resistivity distribution suggests that higher resistivities at the south are related with dried mud materials due to a slightly higher topographical positioning and to the proximity of the slope of the tailings. The northern resistivity distribution is probably related with washout of finer particles increasing porosity, creating a high resistivity zone above schist bedrock. Near the bedrock, lower resistivity distribution can be interpreted as having higher water content and probably an accumulation of upper migrated finer size particles. There is also some minor degree of horizontal to sub-horizontal resistivity changes that are interpreted as material composition changes (mineralogical or/and size distribution) over the mud impoundment.

Spatial relationships are easier in a Geographical Information System (GIS) project. On Figure 11, it is depicted a view with borehole locations (MS4 and MS5), GPR profiles (POS, PES, P9, PO and PE) and ERT sections (L9 and L99).

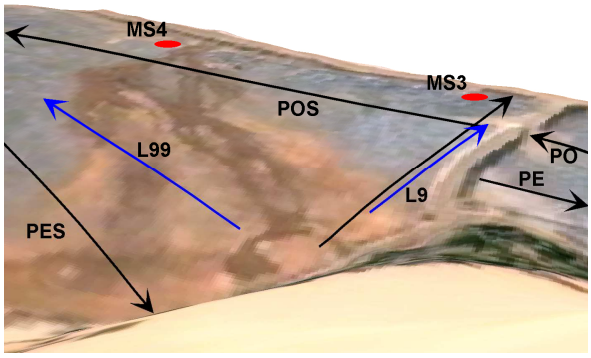

Figure 11: Survey works on actual topography (Same 3D perspective)

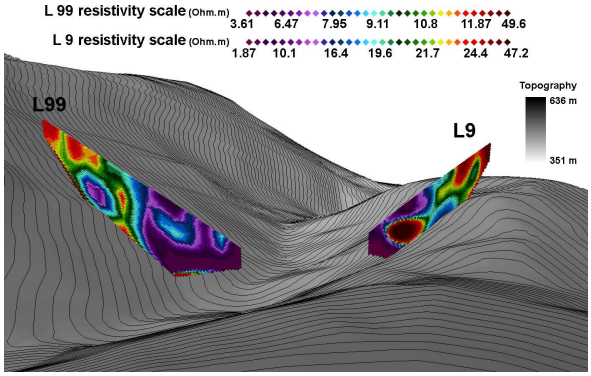

Figure 12: Bedrock topography and ERT resistivity models (Same 3D perspective)

Figure 12 shows the exact same view, without the mud impoundment surface, with resistivity models for L99 and L9 ERT profiles and the bedrock topography digital model. As it can be seen high resistivity values on L99 are bellow the bedrock topography and thus should correspond to the schist bedrock. For both, L99 and L9, resistivity increases with distance from the known position of the water stream, which is in accordance with shallower bedrock. As the lowest resistivity values are modeled over the position of the stream, water content should be higher in this region. Therefore, is likely to be an important seepage pathway and, hence, a risk for the stability of the tailings.

4.2 Geochemical data and interpretation

4.2.1 Grain size

The grain size of the Rio tailing materials is variable, due to successive finer grinding procedures, and is classified as: coarse sterile material from the mine, coarse tailings (sterile material) from the heavy media separation (sand, mud, and slush). The first three types of materials were disposed of on the tailings, but the mud and slush were discharged into a pond specifically constructed for that purpose.

4.2.2 Data from core samples

Selected drill cores were studied macroscopically. The samples revealed vertical zonation, with the upper parts of the cores generally formed by fine dark grey mud while the lower parts (7 to 10 m from the bottom) were reddish, sometimes with greenish grey shades. Ferruginous crusts, 0.1 to 0.8 m thick, were observed in all drill cores. These crusts were yellow, red, and/or brown colours and are probably related to successive dry summers in the past.

Selected trace element composition of the studied drill cores material is given in Table 3. The chemical analysis demonstrates the dominance of As (3094 - 240000 mg kg^{-1}), Cd (28 - 4028 mg kg^{-1}), Cu (78 - 7200 mg kg^{-1}), Fe (5.3 - 28.8%), and Zn (142 - 27000 mg kg^{-1}).

Table 3: ICP-MS results for As, Cd, Cu, Fe, Mn, P, Pb, Sn, W, and Zn for core samples from Rio tailing. Concentrations are expressed in mg kg^{-1} except for Fe (%).

Sample	Depth (m)	As	Cd	Cu	Fe	Mn	P	Pb	Sn	W	Zn
Detection Limit											
MS1/1	2.39	140000	2456	4848	21.4	1605	1509	297	539	7788	11000
MS1/2	10.0	87000	1419	3837	15.0	841	949	116	274	5464	6500
MS1/3	23.0	3094	45	1092	5.3	854	1178	104	584	2232	2199
MS1/4	35.49	19000	207	1477	7.4	786	1302	82	384	2162	2776
MS1/5	40.43	3313	28	78	6.5	419	564	625	400	4071	142
MS2/1	2.73	100000	1985	3834	11.3	1172	2452	97	858	5269	27000
MS2/2	13.48	4332	59	1038	5.8	737	920	143	661	2050	2431
MS2/3	19.58	4786	58	1586	5.4	862	1210	120	560	2676	2292
MS3/1	2.32	190000	2996	2804	18.0	1369	1029	312	869	8676	9100

MS3/2	8.0	240000	4028	7200	28.5	791	449	821	875	6096	21000
MS3/3	16.53	6400	60	1895	6.1	899	1135	103	228	3296	1254
MS3/4	32.0	6800	63	1957	5.4	988	1435	94	425	2637	1143
MS4/1	0.0	220000	3802	873	24.8	795	439	132	411	3728	4185
MS4/2	8.38	180000	3026	4268	28.8	1100	1059	179	832	3754	18000
MS4/3	22.0	6400	57	1895	5.8	852	1077	73	216	3486	1394
MS4/4	32.58	8900	104	1593	6.4	833	1149	182	376	2782	2015
MS4/5	36.0	32000	459	2123	9.8	797	1034	165	433	2989	3907

The results show that, in all cores, As is enriched from the surface down to a depth of 13 m, concentrations ranging from 8.7 to 24%; below this depth, arsenic concentrations decrease to values near or below 1%. The exceptions are cores MS1 and MS4 where the As content increases at 35-36m depths.

4.2.3 Core samples chemical analysis

The Rio tailings samples (MS2 and MS4 – Figure 2) contained abundant amounts of scorodite, sphalerite, wolframite, quartz, natrojarosite, montmorilonite, ilite-vermiculite, some silicates like kaolinite, and also sulphate minerals. Arsenopyrite breaks down through the actions of oxygen, water, and catalytic bacteria (e.g. *ferrooxidans* sp.) in the supergene environment, being scorodite ($FeAsO_4 \cdot 2H_2O$) one of the major products (Boyle and Jonasson 1973; Dove and Rimstidt 1985; Robins 1987). According to Dove and Rimstidt (1985), a typical reaction leading to destruction of arsenopyrite in the supergene environment is:

$$FeAsS + 14Fe^{3+} + 10H_2O \rightarrow 14Fe^{2+} + SO_4^{2-} + FeAsO_4 \cdot 2H_2O + 16H^+$$

During runoff events, rain water infiltrates the tailings and dissolves secondary minerals, producing strongly acidic water. The low pH keeps the trace elements dissolved and increases remobilization and spatial distribution. The chemical composition of these acid effluents is in Table 4.

Table 4: pH, electrical conductivity and trace elements concentrations in seepage waters collected in the Rio tailings (n=11).

Variables	Units	D.L.	SP1	SP2	SP3
pH	-	-	3.0	2.9	3.2
Conductivity	µS cm^{-1}	-	3630	4400	2020
As	µg L^{-1}		2138	544	146
Cd	µg L^{-1}		464	393	226
Cu	µg L^{-1}		42700	54300	20100
Fe	µg L^{-1}		82500	91000	9400
Mn	µg L^{-1}		88700	92600	22300
Ni	µg L^{-1}		2153	2827	1137
Pb	µg L^{-1}		<22	<22	<22
Zn	µg L^{-1}		49200	44500	21900

* These three values are lower then the quantification limit of the ICP-MS method but higher than the detection limit of the samples.

Samples SP1, SP2, and SP3 show pH values typical of acid mine drainage (AMD) waters. The chemical composition of these waters show extremely high concentrations of dissolved sulphate, Al, As, Cd, Co, Cu, Fe, Mn, Ni, and Zn. All of these concentrations exceed the reference limits for water quality. According to the Ficklin diagram (Plumlee et al. 1994) these waters are plotted in the “Acid high-metal” and SW10, SW11 near “High acid/extreme metal” zone (Ávila et al., 2008). The observed metal concentrations are similar to other AMD case studies (Boult et al. 1994; Brake et al. 2001; Sainz et al. 2003; Sracek et al. 2004).

4.2.4 Mud samples chemical analysis

The existing pond at the Rio tailings dam is an open-air impoundment and contains 731034 m^3 of rejected ore concentrates with high metal levels. The Rio dam materials from Barroca Grande also contain high concentrations of As (3094-240000 mg kg^{-1} - in Table 5) and high contents of Cd, Cu, Fe, Mn, Sn and Zn.

Table 5: Rio tailings dam mud samples chemical analysis (values in mg kg^{-1} except Fe %).

Var	D.L.	Rio tailings dam (mud samples)			
		Rio Dam (N=17)			
		Mean	Median	Min	Max
As	20	73649	19000	3094	240000
Cd	4	1227	207	28	4028
Cu	1	2494	1895	78	7200
Fe	0.2	12,45	7,4	5,3	28,80
Mn	50	924	852	419	1605
Pb	16	215	132	73	821
Sn		525	433	216	875
Zn	5	6843	2776	142	27000

The DRX analysis of the Rio dam samples revealed the presence of quartz, mica, feldspar, illite-vermiculite, arsenopyrite, marcasite, pyrite, pyrrhotite, and chalcopyrite. Other minerals like scorodite and natrojarosite are also present.

Table 6 show the distribution of the As, Cu, Fe, Mn, Pb and Zn in selected samples from the Rio mud dam and the Rio tailing according the different granulometric classes. According to the results all the samples show enrichment in As, Cu, Mn, Pb and Zn and they may pose a more significant potential threat due to the fine-grained nature of the materials and its location with respect to Zêzere River. It is also important to realize that these fine materials, stored in the open-air impoundments, can be transported as dust or in suspension by the surface waters and accumulates on solid materials.

Table 6: Selected mud samples granulometric distribution classes for of the As, Cu, Fe, Mn, Pb and Zn.

Sample	As	Cu	Fe %	Mn	Pb	Zn
RD1 – Sample collected in the Rio mud dam near borehole MS4						
Total	190000	250	20,7	361	103	494
RD1 < 32um	290000	1040	20,7	360	128	612
32um<RD1<63um	110000	229	32,9	674	122	110
63um<RD1<180um	59000	335	27,9	500	133	102
180um<RD1<1000um	20000	131	7,4	116	<32	53
RD2 – Sample collected in the Rio mud dam near borehole MS2						
Total	150000	5744	17,6	356	143	3607
RD2 < 32um	200000	8700	19,1	479	272	5300
32um<RD2<63um	170000	4821	24,5	459	171	3297
63um<RD2<180um	120000	8500	19,7	344	150	5200
180um<RD2<1000um	98000	2896	11,6	219	82	2098
TD1 – Sample collected in the Rio tailing near sample RD1						
Total	3729	175	3,5	192	<32	70
TD 1< 2um	42000	700	20	519	461	573
2um<TD1 < 63um	17000	363	11,8	440	182	290
63um<TD1<180um	11000	233	5,9	427	<32	174
180um<TD1<1000um	3839	99	2,9	161	<32	58
1000um<TD1<2000um	2364	82	2,3	135	<32	33
TD2 – Sample collected in the Rio tailing near sample RD2						
Total	1882	229	2,8	166	<32	27
TD 2 < 63um	22000	1476	16,9	483	862	409
63um<TD2<180um	18000	967	9,6	463	152	178
180um<TD2<1000um	3326	178	2,9	178	<32	33
1000um<TD2<2000um	1776	117	2,4	157	<32	<12

An arsenopyrite stockpile, about 9400 m^3, was deposited in the past and remained exposed until June 2006. Then the pile was capped with geotextile and layers of clay (e-EcoRisk 2007). The sample collected from the arsenopyrite stockpile (AST – Figure 2) presents high concentrations of Ag (124 mg kg^{-1}), As (210000 mg kg^{-1}), Cd (3057 mg kg^{-1}), Cu (1426 mg kg^{-1}), Fe (19.8%), Pb (1450 mg kg^{-1}), W (5166 mg kg^{-1}), and Zn (460 mg kg^{-1}) – see Ávila et al., (2008). The presence of several slippage zones in the tailings indicates a risk of collapse and,in this scenario, the arsenopyrite stockpile will enter directly into the Zêzere River.

4.2.5 Geochemistry distribution model.

The element concentration distribution volume models for Ag, As, Cd, Cu, Fe, Mn, Zn and W, are depicted in Figure 13 and Figure 14. These models were limited by surface topography, historical

records of the bedrock topography (Figure 2) and drilling information (Table 2). All data were interpolated and a 3D geochemistry distribution model was produced using Rockworks software.

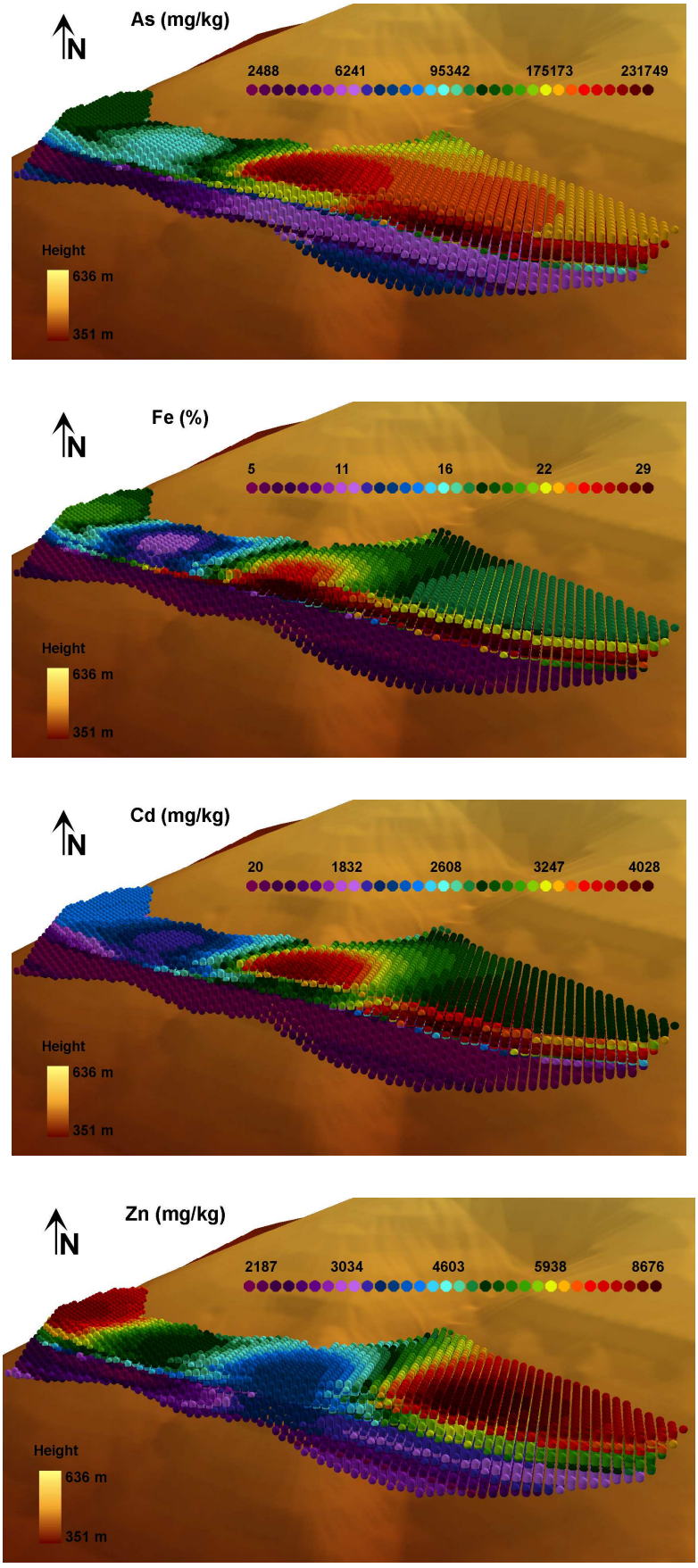

Figure 13: Geochemistry distribution models for As, Fe, Cd, Zn (3D perspective).

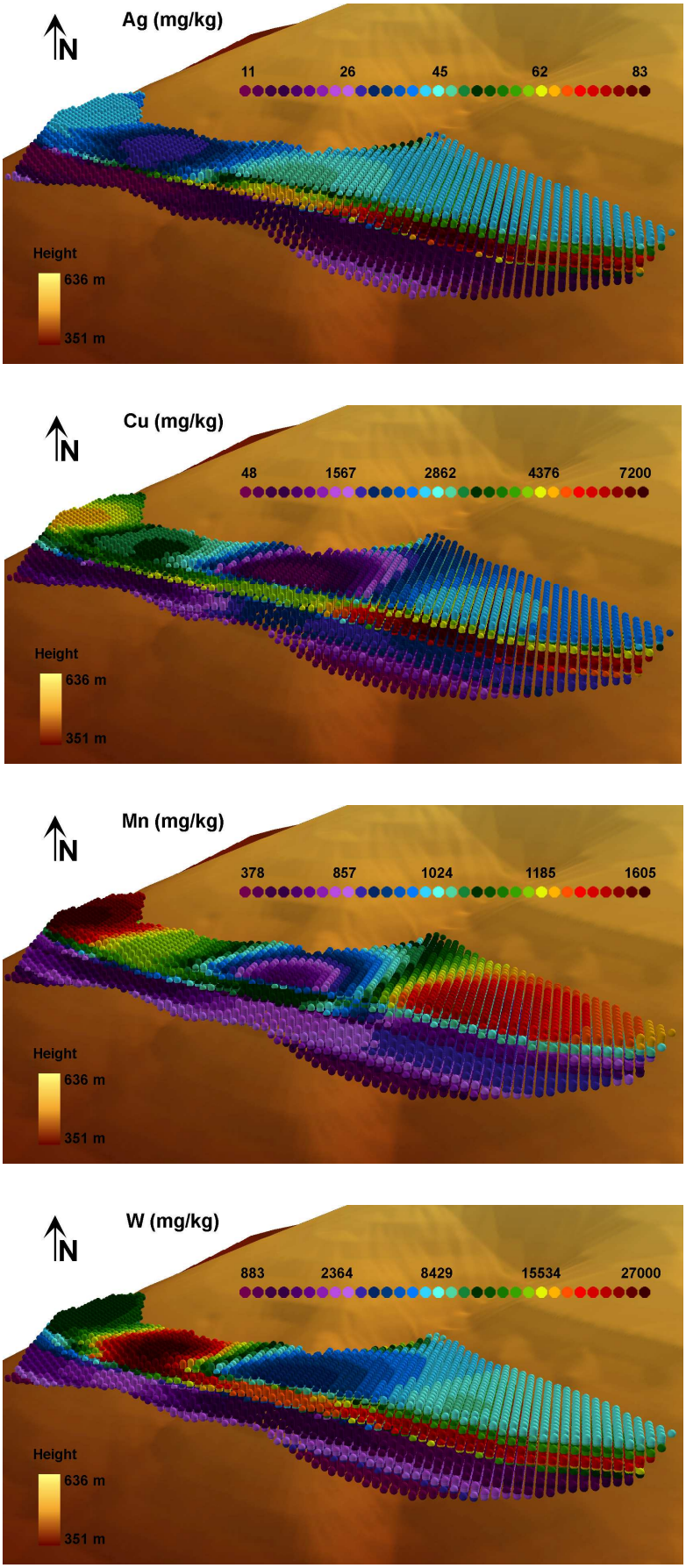

Figure 14: Geochemistry distribution models for Ag, Cu, Mn and Zn (3D perspective).

Historical data show that mine waste materials have different size distribution over the mud impoundment, because of changes of the ore processing technology.

Ore concentrates production contained all the existent heavy minerals, that is, wolframite, cassiterite and sulphides. The sulphides, mainly coarse grain with high metal contents, were considered as sterile material and rejected to the tailings. When the company began to produce copper, these “steriles” sulphides were milled to a fine calibre in order to separate and recover the cooper from the chalcopyrite, but the others sulphides were rejected with the finer calibres. Hence, they became more reactive to rain weathering and leaching and, consequently, they have contributed to the increasing of metals contents in tailings and mud dams (Ávila et al., 2008). Chemical analysis data and particle size distribution from borehole strongly suggests that this geochemical anisotropy is correlated to the element concentration changes at certain depths independently of the borehole location.

The coexistence of wolframite, cassiterite, sulphides, carbonates, and silicates is responsible for the geochemical behavior in the Rio tailings environment. Weathering of sulphide-rich materials results in AMD formation. During dry seasons, these acidic waters evaporate, progressively depositing sulphate efflorescences which is a characteristic of an extremely acidic environment. These are rarely found as mono-mineral phases. In fact, most consist of mixtures of Fe-Al hydrated sulphates such as melanterite and minor amounts of rozenite and szomolnokite. In Rio tailing dam the presence of melanterite ($Fe^{2+}(SO_4)\cdot 7(H_2O)$) and minor amounts of rozenite ($Fe^{2+}(SO_4)\cdot 4(H_2O)$) and szomolnokite ($Fe^{2+}(SO_4)\cdot(H_2O)$) were observed (DRX identification). This new mineralogy is mainly controlled, Frau (2000) and Valente and Leal Gomes (1998), by the wet–dry cycles related to seasonal variations in rainfall. These neoformation mechanisms limit the downstream effects of the acid drainage since the crusts and clays efficiently fixate some of the contaminant elements, especially the iron oxides (Valente and Leal Gomes 1998). The ferruginous crust collected at the base of the Rio tailings dam also had high levels of Fe, Cu, Zn, Cd, and As (As = 40 000 mg kg^{-1}; Cd= 453 mg kg^{-1}; Cu = 3,305 mg kg^{-1}; Fe = 12%; Mn = 572 mg kg^{-1}; Pb = 319 mg kg^{-1}; Zn = 663 mg kg^{-1}) and confirms the transfer of these elements from the tailings and mud impoundment.

5. Geophysical and geochemical and information

Geophysical data cell spatial resolution, for GPR and ERT, has higher resolution than that for each geochemistry model. Over the mud impoundment GPR data, due to high attenuation, is too shallow for direct comparison with the geochemistry 3D models, therefore, no direct comparison and discussion is made.

However comparisons can be done between geochemistry and resistivity model data.

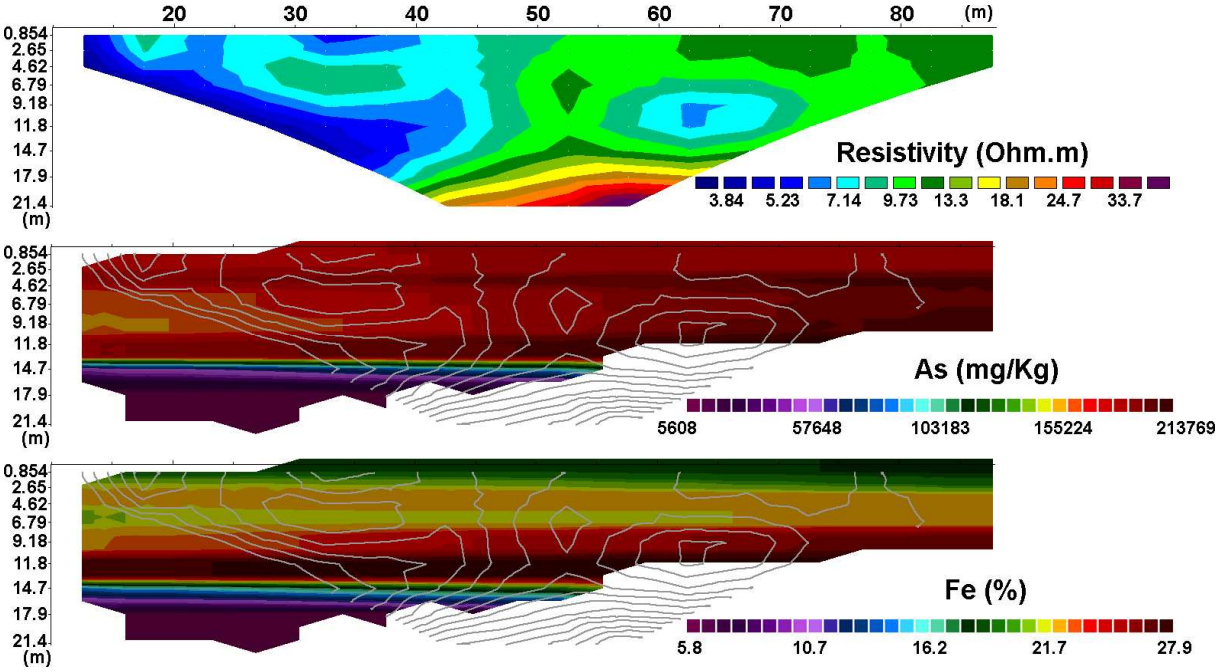

Figure 15: L99 resistivity model (top), superposition of the L99 resistivity model distribution over the As cross section geochemistry model (centre) and over the Fe cross section geochemistry model (bottom).

Resistivity inversion model data (L99), shown on top of Figure 15, is overlapped and compared with sections for the As and Fe geochemical 3D model sections, centre and bottom of Figure 15. The proposed geochemistry models show vertical and lateral heterogeneity that are in close agreement with superimposed lines of equal resistivity. It is possible to identify clearly lateral changes in element concentration that follow the resistivity signatures closely. Lower concentrations at the right side of the elements model sections are at the same position as the lower resistivities. The proximity of the water line has influence on the observed resistivity lower values, possibly due to higher water content. However it is possible to observe horizontal resistivity variations that match elements concentration variation.

Major vertical changes in elements concentration are in agreement with major resistivity changes. At about 3 m depth, for both geochemistry section models, there is a gentle change that is also observed in resistivity distribution. To the top of this smooth boundary, resistivity exhibits a continuous horizontal pattern. Beneath it resistivity shows greater variations, but a general horizontal resistivity distribution remains. To the bottom of the sections, at about 11 m, on left side of Figure 15, until 9 m, right Figure 15, it is possible to observe an increase on the concentration values. This signature is also observed in resistivity.

In spite of the major concentration changes observed for the geochemical models at greater depths, bedrock proximity, limits of the mud impoundment, and lack of lateral resistivity data information has made impossible to obtain a clear resistivity response signature.

6. Conclusions

This study demonstrates the usefulness of an integrative study of Rio tailings clearly. It was possible to investigate the internal structure of the tailings, its geochemical distribution and associated mud (particle size) distribution. Spatial relationships between the overall data were also achieved.

More specifically:

1) GPR was able to map shallow subsurface stratigraphy in the mud impoundment and in the tailings slope. It was possible to differentiate major bounding surfaces, strata sets, and horizontal bedding. Interpreted rest angles are in agreement with those observed in vertical rupture sections in the tailings. The bedrock limit, at the lowest part of the tailings, was also delineated. Attenuation in the GPR signal is larger in the mud impoundment and limits penetration depths.

2) ERT was able to detect bedrock limits on the mud impoundment. It was identified an area of very low resistivity, near the interpreted bedrock and coincident with a steep, mud fulfilled, not permanent stream. There is also an area of high resistivity positioned above low resistivity on the L9 ERT resistivity section. Hence, the presence within this context of high mud volume, low resistivity, possibly indicating higher water content and small size particle migration aggravated by seasonal rainfall collected upstream, puts this area of the Rio tailings in a high endangerment risk. Thought different cell size model comparison, ERT resistivity sections are in close agreement with the 3D expected material size distribution and related geochemical element distribution.

Geochemistry

GIS platform project provided visualization of topographic data, 2D Geophysical (GPR and ERT) 3D geochemical model and expected particle size distribution relationships and helped during interpretation stages. It is a platform for a better spatial understanding of the Rio tailings impoundment system and is a tool for future works on monitoring and management of this complex system.

7. Acknowledgments

This research was funded by the European Commission through the e-Ecorisk Project (# EVG1-2002-25 0068), “A regional enterprise network decision-support system for environmental risk and disaster management of large-scale industrial spills”.

8. References

Almeida, MS (2003) Pavimentos Rodoviários de baixo custo com emulsões betuminosas e resíduos das Minas da Panasqueira. Tese de Mestrado em Engenharia Civil, Universidade da Beira Interior, Covilhã.

ASTM (American Soc for Testing Materials) (1984) Annual Book of ASTM Standards, Water Environmental Technology, v 11.01

Ávila PF, Ferreira da Silva E, Salgueiro AR, Farinha JA (2008) Geochemistry and Mineralogy of Mill tailings impoundments from the Panasqueira mine (Portugal): implications for the surrounding environment. Mine Water Environ 27: 210-224.

Bloot C, de Wolf LCM (1953) Geological features of the Panasqueira tin-tungsten ore occurrence (Portugal). Bol Soc Geol Port 11(1): 1-58

Boult S, Collins ND, White KN, Curtis CD (1994) Metal transport in a stream polluted by acid mine drainage - the Afon Goch, Anglesey, UK. Environ Pollut 84: 279–284

Boyle RW, Jonasson IR (1973) The geochemistry of arsenic and its use as an indicator element in geochemical prospecting, J Geochem Explor 2: 251–296

Brake SS, Connors KA, Romberger SB (2001) A river runs through it: impact of acid mine drainage on the geochemistry of West Little Sugar Creek pre- and post- reclamation at the Green Valley coal mine, Indiana, USA. Environ Geol 40: 1471–1481

Breiter K (2001) Report about Laboratory Investigations of Rock Samples from the Panasqueira Mine and Recommendations for Future Exploration, Nov 2001

BRGM – Management of mining, quarrying and ore-processing waste in the european union. European Commission, DG environment, 50319-FR, 2001

Campbell, D.L., Horton, R.J., Beanland, S., 2000. Geoelectrical Laboratory Measurements of Materials from May Day Mine Dump, Southwestern Colorado: U.S. Geological Survey Open-File Report 00-382, 27 p.

Campbell, D.L., Horton, R.J., Bisdorf, R.J.,Fey, D.L., Powers, M.H., & Fitterman, D.V., 1999. Some geophysical methods tailings/mine waste work. Tailings and mine waste ’99. Proceedings of the sixth international conference, Fort Collins, Colorado, January, 24–27, 1999.

Campbell, D.L. & Fitterman,D.V.2000. Geoelectrical Methods for Investigating Mine Dumps. In: International Conference on Acid Rock Drainage (ICARD2000), May21–24,2000,Denver, Colorado.

Proceedings from the Fifth International Conference on Acid Rock Drainage 2. Colorado: The Society for Mining, Metallurgy, and Exploration Inc., 1513–1523.

Cavey G, Gunning D (2006) Updated technical report on the Panasqueira mine, Distrito de Castelo Branco, Portugal. OREQUEST, 67pp

Conde LN, Pereira V, Ribeiro A, Tadeu D (1971) Jazigos hipogénicos de estanho e volfrâmio. Livro-guia da Excursão #7, I Congresso Hispano-Luso-Americano de Geologia Económica, Lisboa- Madrid, 81 pp

Correa A, Naique RA (1998) Minas Panasqueira, 100 Years of Mining History paper presented at the 1998 International Tungsten Industry Association (ITIA) conference.

Corrêa de Sá A, Naique RA, Nobre E (1999) Minas da Panasqueira – 100 anos de História. Bol de Minas 36(1): 3-22

Davies, M.P., Lighthall, P.C., Rice S., Martin T.E., 2002. Design of Tailings Dams and Impoundments. Tailings and Mine Waste Practices, SME, AGM, Phoenix, 18p.

Dinis da Gama C (2002) Geotechnical and laboratory study of the tailings in the River Zêzere waste heap. Beralt Tin and Wolfram Report, Lisbon, Portugal, 9 pp

Dold B, Fontboté L (2001) Element cycling and secondary mineralogy in porphyry copper tailings as a function of climate, primary mineralogy and mineral processing. Special Issue: Geochemical studies of mining and the environment, J Geochem Explor 74(1-3): 3-55

Dove PM, Rimstidt JD (1985) The solubility and stability of scorodite, $FeAsO_4 \cdot 2H_2O$. Am Mineral 70: 838-844

e-Ecorisk (2007) A Regional Enterprise Network Decision-Support System for Environmental Risk and Disaster Management of Large-Scale Industrial Spills. WP3-case study characterisation. Deliverable 3.1, 20 pp

e-EcoRiskDoW (2001) Regional Enterprise Network Decision-Support System for Environmental Risk and Disaster Management of Large-Scale Industrial Spills. EU project co-ordinated by C. Banninger, 70 pp

Ebraheem, A.M., Hamburger, M.W., Bayless, E.R., Krothe, N.C., 1990. A Study of Acid Mine Drainage Using Earth Resistivity Measurements. Ground Water, Vol.28, No.3, pp. 361-368(7).

Eurostat, Theme 8 Environment and Energy - Waste generated and treated in Europe. Data 1990-2001. 2003.

Farinha JA (2005) Packing and sealing of the sulphides existent on Rio tailing, environmental concerns. Internal Technical Note, April 2005, 5 pp + Appendixes Forstner U, Wittmann GTW (1983) Metal Pollution in the Aquatic Environment. 2nd rev, 24th Edit, Springer-Verlag, Berlin, Germany, 486 pp

Frau F (2000) The formation-dissolution-precipitation cycle of melanterite at the abandoned pyrite mine of Genna Luas in Sardinia, Italy: environmental implications. Mineral Mag 64: 995-1006

Hammond, A – Mining and quarrying wastes: a critical review. Engineering Geology 25 (1988) 17-31.

Julivert F, Fontboté J, Ribeiro A, Conde L (1974) Mapa Tectonico de la Península Ibérica y Baleares, escala 1:1,000,000. Inst Geol Minero España, Madrid, Spain, 113 pp

Kelly WC, Rye RO (1979) Geologic, fluid inclusion and stable isotope studies of the tin-tungsten deposits of Panasqueira, Portugal. Econ Geol 74: 1721-1822

Loke, M.H., 2000. Electrical imaging surveys for environmental and engineering studies, A practical guide to 2-D and 3-D surveys, p. 59. http://www.geoelectrical.com.

Loke MH, Barker RD (1996) Rapid least-square inversion of apparent resistivity pseudosections by a quasi-Newton method. Geophysical Prospecting 44: 131–52.

Lotze F (1945) Observation respect a la division de los variscides de la Meseta Ibérica. Publ Estrag Geol Espanã 5: 149-166.

Nordstrom DK, Alpers CN (1999) Negative pH, efflorescent mineralogy, and consequences for environmental restoration at the Iron Mountain Superfund site, California. Proc, Natl Acad Sci USA 96: 3455-3462

Noronha F, Doria A, Dubessy J, Charoy B (1992) Characterization and timing of the different types of fluids present in the barren and ore veins of the W-Sn deposit of Panasqueira, Central Portugal. Miner Deposita 27: 72-79

Plumlee GS, Smith S, Ficklin WH (1994) Geoenvironmental Models of Minerals Deposits and Geology-based- Mineral–environmental Assessments of Public Lands. USGS Open-File Report 94–203

Panthulu, T.V., Krishnaiah, C., Shirke, J.M., 2001. Detection of seepage paths in earth dams using self-potential and electrical resistivity methods. Engineering Geology 59, 281-295, 15 p.

Poisson, J., Chouteau, M., Aubertin, M., Campos, D., 2009. Geophysical experiments to image the shallow internal structure and the moisture distribution of a mine waste rock pile. Journal of Applied Geophysics 67 (2009) 179–192, 14 pp.

Puura, Eric; Marmo, Luca; Alessandro, Marco - Mine and quarry waste - the burden from the past. Directorate General Environment of the European Commission, Iatly, 2002

Reis AC (1971) As Minas da Panasqueira. Bol. de Minas 8(1): 3-34

Robbins RG (1987) The solubility and stability of scorodite, $FeAsO_4 2H_2O$ (Discussion). Am Mineral 72: 842–844

Rodrigues Abrantes J, Gonzalez V (1973) O tratamento mecânico do minério nas Minas da Panasqueira. Bol de Minas 19(4): 239-247

Sainz A, Grande JA, de la Torre ML (2003) Odiel River, acid mine drainage and current characterisation by means of univariate analysis. Environ Int 29: 51–59

Sjödahl P., Dahlin T. and Johansson S. (2007) Detection of Internal Erosion and Seepage Using Resistivity Monitoring, WasserWirtschaft, 10: 54-56.

Sjödahl, P., Dahlin, T., Johansson, S. (2005). Using resistivity measurements for dam safety evaluation at Enemossen tailings dam in southern Sweden. Environmental Geology 49, 267–273.

Sracek O, Choquette M, Gélinas P, Lefebvre R, Nicholson RV (2004) Geochemical characterization of acid mine drainage from a waste rock pile, Mine Doyon, Quebec, Canada. J Contam Hydrol 69: 45–71

Valente T, Leal Gomes C (1998) Tipologia e evolução dos materiais de neoformação supergénica detectados na escombreira da Mina de Valdarcas (Vila Nova de Cerveira – N Portugal) –Implicações ambientais. Cadernos Lab, Xeológico de Laxe 23: 43-58

Van Dam, R.L., Gutierrez L.A., McLemore V.T., Wilson G.W., Hendrickx J.M.H., Walker B.M., 2005. Near Surface Geophysics for the Structural Analysis of a Mine Rock Pile, Northern New Mexico. ASMR, National Meeting of the American Society of Mining and Reclamation, 1178-1221, 24pp.

Vanhala, H., Räisänen, M.L. Suppala, I., Huotari, T., Valjus, T. and Lehtimäki, J., 2005. Geophysical Characterizing of Tailings Impoundment - A Case From the Closed Hammaslahti CU-Zn Mine, Eastern Finland. Geological Survey of Finland, Special Paper 38, 49– 60, 2005. http://arkisto.gtk.fi/sp/sp38/sp38_pages_49_60.pdf

Yuval D.W.O., 1996. DC resistivity and IP methods in acid mine drainage problems: results from the Copper Cliff mine tailings impoundments. Journal of Applied Geophysics, Volume 34, Number 3, April 1996, pp. 187-198(12).

Watson M.I., Locke C.A., Cassidy J., 2001. Imaging of Mine Tailings Leachate Using Ground Penetrating Radar and Electromagnetic Methods at Tui Mine, New Zealand. EAGE, 63rd Conference and Technical Exhibition -, Amsterdam, The Netherlands. M-003, 4p.